Original Research Paper

A biomimetic antitumor nanovaccine based on biocompatible calcium pyrophosphate and tumor cell membrane antigens

Minghui Li[1], Mengmeng Qin[1], Ge Song, Hailiang Deng, Dakuan Wang, Xueqing Wang, Wenbing Dai, Bing He*, Hua Zhang*, Qiang Zhang*

Beijing Key Laboratory of Molecular Pharmaceutics and New Drug Delivery Systems, State Key Laboratory of Natural and Biomimetic Drugs, School of Pharmaceutical Sciences, Peking University, Beijing 100191, China

ARTICLE INFO

ABSTRACT

Currently, the cancer immunotherapy has made great progress while antitumor vaccine attracts substantial attention. Still, the selection of adjuvants as well as antigens are always the most crucial issues for better vaccination. In this study, we proposed a biomimetic antitumor nanovaccine based on biocompatible nanocarriers and tumor cell membrane antigens. Briefly, endogenous calcium pyrophosphate nanogranules with possible immune potentiating effect are designed and engineered, both as delivery vehicles and adjuvants. Then, these nanocarriers are coated with lipids and B16-OVA tumor cell membranes, so the biomembrane proteins can serve as tumor-specific antigens. It was found that calcium pyrophosphate nanogranules themselves were compatible and possessed adjuvant effect, while membrane proteins including tumor associated antigen were transferred onto the nanocarriers. It was demonstrated that such a biomimetic nanovaccine could be well endocytosed by dendritic cells, promote their maturation and antigen-presentation, facilitate lymph retention, and trigger obvious immune response. It was confirmed that the biomimetic vaccine could induce strong T-cell response, exhibit excellent tumor therapy and prophylactic effects, and simultaneously possess nice biocompatibility. In general, the present investigation might provide insights for the further design and application of antitumor vaccines.

1. Introduction

For the past few years, cancer immunotherapy has become the fourth pillar of cancer treatment, which is complementary to surgery, chemotherapy and radiation therapy [1]. Traditional tumor treatment methods such as surgery and chemotherapy, with disadvantages such as poor specificity and strong adverse reactions, could not reach the satisfying level in curing tumors. Immunotherapy inhibits tumors by training

and stimulating the host immune system [2,3], showing unique advantages. Tumor immunotherapy exhibits strong specificity, long-lasting effect, lower toxicity, less off-target effects [4,5], and good curative effect in clinical, in terms of checkpoint blocked therapy, adoptive cell therapy (ACT) and cancer vaccination. Checkpoint blocked therapy can produce a durable response, but its clinical benefit is limited to a small number of patients, partially because of insufficient T cell infiltration in the tumor environment [6–8]. ACT can sometimes be life-threatening and require a mass of cost and time [9,10]. As one of the most developed parts of immunotherapy, therapeutic cancer vaccines can trigger a cytotoxic T lymphocytes (CTLs) response [11], which have made great progress, especially in the development of personalized cancer vaccines [12,13]. However, in the construction of vaccines, the selection of effective antigen and suitable adjuvants still remains to be a huge challenge [14].

The design of an effective vaccine includes the following three parts: (a) antigens that can cause the body to produce specific immune responses; (b) immune adjuvants which stimulate innate immunity to enhance the immune effect; (c) targeted delivery systems that can enhance antigen presentation and adjuvant effect [15]. Peptide vaccines are relatively simple, safe and easy to be produced [13], but still require identification and manufacturing of tumor antigens [11] and those peptide vaccines have a short half-life and are difficult to reach the antigen-presenting cells (APCs) [16]. With the development of sequencing technology, vaccines based on tumor neoantigens have shown good clinical efficacy [17], but the identification and selection of neoantigens remains challenging [18]. Biomimetic tumor vaccines outsourcing cell membranes have shown more potential without the need for sequencing or antigen synthesis [19], and cell membrane coating technology breaks through the limitations (quickly eliminated in circulation) of ordinary nano systems. CTLs usually recognize tumor cells by binding to receptors on cancer cell membranes [20]. Tumor cell membranes contain a large number of tumor antigens, they can specifically activate cellular immune response compared with the whole cell lysates, and multiple antigens on cell membranes will cooperate with each other to trigger a powerful immune response. In consequence, the development of cancer vaccines using tumor cell membranes as tumor-specific antigens shows great potential.

Besides antigens, adjuvants can be activators for APCs to form an immune response [21]. An ideal vaccine adjuvant should provide a sufficient amount of antigen at the appropriate site and concentration, increase the production of costimulatory molecules, and produce stimulating cytokines [22]. Traditional immune adjuvants such as aluminum adjuvants have been widely applied, but their safety remains controversial [23,24]. Aluminum adjuvant can only activate humoral immunity and hardly stimulate T helper cell type 1 immune response [25,26]. Currently, using nanoparticles themselves as vaccine adjuvants provides us with a new perspective [27]. To date, various nanoparticles have been developed as delivery vehicles for immunogens in vaccines.

Among them, calcium phosphate nanoparticles (CaP-NPs) are the most promising and have been studied as immune adjuvants [28,29]. As nanomaterials, CaP-NPs can increase the delivery and uptake efficiency of antigens. Thus, the accumulation of antigens in APCs is increased, which has been extensively studied in vaccine delivery [30–34]. Besides, CaP-NPs have potentials to function as adjuvants for inducing more balanced T helper cell type 1 (Th1) and T helper cell type 2 (Th2) based immune responses [35]. Studies have shown that CaP-NPs can activate NLRP-3 inflammasome, and subsequently stimulate the production of cytokines such as IL-1β as a co-activator to promote various types of T cell based responses [22,36]. As a type of acid-sensitive materials, CaP-NPs can rapidly dissolve in acidic lysosome or endosome environments and release the drug, providing an ideal matrix for antigen peptides release [37]. The calcium phosphate system has shown great potential as antigen delivery system and immunopotentiator to construct a simple and effective vaccine.

Various nanoparticles are used as drug delivery vehicles, such as polymer conjugates, polymer nanoparticles, lipid-based carriers, gold nanoparticles and so on [27,38]. However, the biocompatibility and toxicity of these nanoparticles are tremendously different, on account of their inherent differences in physical properties (size, shape, etc.) and chemical characteristics (surface chemistry, hydrophobicity, etc.), preparation methods and their biological targets (cells, tissues, organs, animals, etc.) [39–42]. Therefore, discovering nanomaterials with good biocompatibility and high safety for drug delivery is an important direction of current drug delivery system design. Using substance or elements contained in the organism itself is one way to address the biocompatibility issue [43]. Calcium phosphate, as a biodegradable and biocompatible material, is the main component of human bones and teeth. It has been widely used and studied in bone and tooth restoration applications, and can be well tolerated and easily regenerated [44]. Composite nanoparticles based on calcium phosphate are further proved to be potent candidates for the treatment and imaging [45–49]. The calcium phosphate is considered to be safe by FDA, and previous researches have shown that calcium phosphate nanoparticles have not shown significant toxicity on any cell lines [50]. Similarly, calcium pyrophosphate is also a substance that exists in our body, which is diffusely present in plasma and matrix [43,50]. Previous studies have used such materials as drug delivery vehicles and demonstrated their advantages [43,51,52].

Here, we construct a calcium pyrophosphate nanovaccine coated with cell membrane (CM@CaPyro). The CaPyro nanogranules was designed both as a delivery vehicle and an immune adjuvant. The B16-OVA tumor cell membrane which contains multiple tumor antigens was modified on the surface of the nanogranules. The CaPyro nanogranules are also covered with artificial phospholipid bilayers, which are combined with the tumor cell membrane in a self-assembling manner to achieve effective payload of antigens and to be efficiently delivered to APCs for activating specific cellular immunity. The "proof of concept" study was then conducted *in vitro* and *in vivo*.

2. Materials and methods

2.1. Materials and animals

CaCl$_2$•2H$_2$O was purchased from Xilong Scientific (Guangzhou, China), sodium pyrophosphate was obtained from Aladdin (Shanghai, China), 1,2-dioleoyl-sn- glycerol - 3-phosphate (sodium salt) (DOPA) and NBD-PE were bought from Avanti Polar Lipids, Inc. (Alabama, USA). 1,2-distearoyl-sn–glycero-3-phosphoethanolamine polyethylene glycol 2000 (DSPF-PEG) was purchased from NOF Corporation (Kawasaki, Japan). 1,2-Dioleoyl-sn–glycero-3-phosphocholine (DOPC) was obtained from TCI (Shanghai, China). 1 M Tris–HCl buffer (pH 7.0) was the product of from BioRoYee (Beijing, China). Rabbit monoclonal to Melanoma gp100 and Rabbit monoclonal to Calreticulin were bought from Abcam (Cambridge, British). DCT rabbit polyclonal antibody was obtained from Proteintech Group, Inc (Chicago, USA). lipopolysaccharides (LPS) was purchased from Shanghai yuanye Bio-Technology Co., Ltd (Shanghai, China). CFSE was obtained from TargetMol (Shanghai, China). APC anti-mouse CD3, PE/Cy7 anti-mouse CD4, AF488 anti-mouse CD8α, APC anti-mouse CD11c, PE/Cy7 anti-mouse CD80, PE anti-mouse CD86 were purchased from Biolegend (San Diego, USA). ANTI-MO SIINFEKL (25-D1.16) PE was obtained from eBioscience (San Diego, USA). Dulbecco's modified eagle medium (DMEM) and Roswell Park Memorial Institute 1640 containing GlutaMax medium (RPMI 1640) were bought from MACGENE Biotechnology Ltd (Beijing, China). Lyso-tracker was obtained from Thermo Fisher Scientific Inc (Waltham, MA, USA). Other reagents were all analytical grade. C57BL/6 mice (5–8 weeks) were obtained from Peking University Health Science Center Department of Laboratory Animal Science (Beijing, China). All animal experiments were performed according to the rules of Experimental Animals Administrative Committee of Peking University.

2.2. B16-OVA murine melanoma cell culture and membrane derivation

B16-OVA mouse melanoma cells were cultured at 37 °C with 5% CO$_2$ in T75 tissue culture flasks with DMEM supplemented with 10% bovine growth serum (Genimi) and 1% penicillin-streptomycin. At 80%−90% confluency, 8–10 million cells per flask were collected in blank DMEM by scraping, pelleted at 1500 rpm for 5 min, then resuspended in a membrane extraction buffer containing 30 mM Tris–HCl pH 7.0 with 0.0759 M sucrose and 0.225 M D-mannitol with 1% PMSF [53]. Next, the cell suspension was repeatedly frozen and thawed for 3 times in liquid nitrogen, and then further broken by ultrasound at 100 W for 30 min in an ice bath. Homogenate was pelleted at 600 g and 4 °C for 10 min, and the supernatant was then pelleted at 8000 g and 4 °C for 10 min. Then the supernatant collected again was centrifuged 15,000 rpm, 4 °C for 30 min to collect the pellet. The pellet was resuspended in membrane extraction buffer and stored at −20 °C until use. Total membrane protein content was quantified by BCA protein assay kit.

2.3. Nanogranule preparation

The CaPyro cores were prepared via a water-in-oil microemulsion method as previously described [52]. A microemulsion was prepared by the addition of 50 mM Na$_2$H$_2$P$_2$O$_7$ aqueous solution (50 µl) and 500 mM CaCl$_2$•2H$_2$O solution (50 µl) to separate 4 ml mixed solvent as previously described [52] while vigorously stirring at room temperature. 160 µl DOPA solution (14.46 mg/ml in CHCl$_3$) was added to pyro-phosphate's reaction system and the stirring was continued for 30 min until a clear solution formed. The two microemulsions were combined and the mixed microemulsion was stirred for 30 min at room temperature. Then twice the volume of ethanol was added and stirred for 20 min. Next, the liquid was centrifuged at 10,000 rpm for 10 min. The pellet was washed three times as described in early research [52], and re-dispersed in tetrahydrofuran (THF).

As previous research described [52], CaPyro cores were prepared by adding a THF solution of 1,2-distearoyl-sn–glycero-3-phosphocholine, DSPF-PEG and DOPA-coated CaPyro cores to 1 ml of 30% (v/v) ethanol/water (ethanol/PBS, when used in cells or animals) at 50 °C. The mixture was stirred at until THF and ethanol were completely evaporated. Then, the CaPyro solution was obtained. B16-OVA cell membrane solution which contained 10 µg cell membrane proteins was added into CaPyro solution and the mixture was sonicated by ultrasound at 100 W, 50 °C for 30 min. With that, completed CM@CaPyro nanogranules were obtained. For the preparation of Imject Alum/CM, 60 µg cell membrane proteins were added into 300 µl PBS, and then the solution was mixed with 300 µl Imject Alum Adjuvant (Thermo Fisher Scientific, Shanghai, China) and stirred at 500 rpm, 30 min.

2.4. Physical characterization

The size and zeta potentials of CaPyro and CM@CaPyro NGs were determined by dynamic light scattering (DLS) using a Zetasizer Nano ZS (Malvern Panalytical, Malvern, British) and the morphology was examined under a field emission transmission electron microscopy (TEM) (JEM1400PLUS, Japan).

2.5. Loading capacity and efficiency of cell membrane

The nanogranules were lysed on ice with cell lysis buffer for Western and IP for 15 min before measuring protein concentration. Then the mixture was centrifuged at 10 000 rpm and 4 °C. The supernatant was collected. The amount of cell membrane on the nanogranules was determined by the Bradford method. To determine the lyophilized quality of the formulations, the formulations were frozen at −80 °C, then lyophilized and weighed.

2.6. Membrane antigen retention and identification

Identification of characteristic B16-OVA tumor antigens was completed via SDS- PAGE and western blotting. B16-OVA cells were lysed to prepare the whole cell lysate as a positive control. Equivalent 10 µg of protein per sample

was loaded into each well of a 10% Tris/glycine SDS-poly-acrylamide gelatin in an electrophoresis chamber system (Bio-Rad Laboratories, PA, USA) and run at 120 V for 100 min. For total protein imaging, the protein blots were stained with Coomassie Blue Fast Staining Solution (Beyotime Biotechnology, China). For western blot analysis, the protein was transferred to polyvinylidene fluoride membranes (Millipore, Massachusetts, America) which were then blocked with QuickBlock^{TM} blocking buffer (Beyotime Biotechnology, Shanghai, China) for 30 min at 37 °C. The blots were detected by antibodies against gp100, Trp2 (DCT) and calreticulin overnight at 4 °C. And then incubated with the horseradish peroxidase-conjugated anti-rabbit IgG (Beyotime Biotechnology, Shanghai, China) before the final visualization on film. The protein bands of gels and PVDF membranes were imaged by Tanon 5200 Multi automatic chemiluminescence/fluorescence image analysis system (Shanghai, China).

2.7. Cytotoxicity of nanovaccine in DC 2.4 cells

The cytotoxicity of blank and completed nanogranules was tested in DC 2.4 cells. The cells were seeded on 96-well plates at 8000 cells per well. After incubating for 24 h, the cells were treated with free sodium pyrophosphate, CaPyro NGs and CM@CaPyro NGs for 24 h. The cells without treatment served as controls. The cell viability was detected by CCK-8 assay.

2.8. Intracellular uptake of DC 2.4 and BMDCs

DC 2.4 cells were planted on 12-well plates at 1×10^5 cells per well and incubating for 24 h. Bone marrow-derived dendritic cells (BMDCs) were isolated from C57BL/6 mice and cultured in RPMI-1640 medium containing GM-CSF (200 U/ml), with regular replenishment of fresh medium on Day 2 and Day 4 [7,31]. On Day 6, BMDCs were collected by centrifugation and re-seeded in 12-well plates. DC 2.4 cells or BMDCs were incubated with NBD-PE-labeled CM and NBD-PE-labeled CM@CaPyro NGs at different times, different concentrations or at different temperatures. Then the cells were collected and analyzed by flow cytometry. For confocal experiments, the cells were washed 3 times with PBS and incubated with 50 mM Lyso Tracker Red DND-99 (Invitrogen, California, America) for 30 min to label lysosome and 1 × Hoechst 33,342 Staining Solution for Live Cells (Beyotime Biotechnology, Shanghai, China) to label nucleus. Then the cells were imaged under confocal microscopy.

2.9. BMDCs maturation and antigen presentation

BMDCs were cultured for 6 d as described above. On Day 6, immature BMDCs were seeded in 12-well plates at 1×10^6 cells per well, and the formulations were added to the culture solution at a final concentration of CM@CaPyro (400 µg/ml), CM (contained equivalent dosage of cell membrane proteins of nanogranules), LPS (10 µg/ml, as a positive control), and incubated for 24 h at 37 °C. Subsequently, BMDCs were collected, and supernatant was collected and stored at −20 °C for enzyme-linked immunosorbent assay (ELISA) to measure the concentration of TNF-α and IL-12p70. And then

the cells were washed with PBS and stained on ice with fluorescently labeled antibodies against CD11c, CD80, CD86. Cells were then carefully washed for 3 times by using PBS and analyzed by flow cytometry. For the antigen presentation assay, BMDCs was stained with APC-labeled anti-mouse SIINFEKL/H-2Kb monoclonal antibody 25-D1.16 and analyzed by flow cytometry. The data were analyzed by FlowJo 7.6.

2.10. In vivo activation of dendritic cell and T cell response

The immunization schedule is the same as the therapeutic anti-tumor experiment. Then the immunized mice were sacrificed on Day 14 to obtain draining lymph nodes (LNs), spleens and peripheral blood, and the remaining mice were sacrificed on Day 21 to get tumors. Tissues mentioned above were processed into a single cell suspension and then diluted to a concentration of 1×10^7 cells/ml. Each sample contained 100 µl suspension, and were stained with fluorescently labeled antibodies against CD11c, CD80, CD86, CD3, CD4, CD8α. Then the samples were detected by flow cytometry.

2.11. Evaluation of lymph node retention by living imaging

C57BL/6 mice were subcutaneously injected with DiR-labeled CM@CaPyro NGs (1.5 mg per mouse). Mice were sacrificed at 4, 12, 24, 48, 96 and 168 h. Then alar lymph nodes and major organs were obtained. These tissues were analyzed by *in vivo* living imaging (IVIS SPECTRUM, Perkinelmer, America).

2.12. Immunization for therapeutic anti-tumor treatment

2×10^4 B16-OVA cells were subcutaneously injected into the left armpit of C57BL/6 mice (5–8 weeks) on Day 0, and the mice which were randomly divided into 4 groups ($n = 6$) were immunized as follows: the mice were subcutaneously injected in back with 100 µl of saline, CM@CaPyro (1.5 mg/100 µl, contains 10 µg CM proteins), CaPyro (1.5 mg/100 µl), CM and Imject Alum/CM (equivalent proteins dosage to nanovaccine). Then the immunized mice were monitored for tumor growth and body weight. The tumor volume was estimated using the following formula: width^2 × length × 0.5. Tumor growth was measured at 2-d intervals.

2.13. Immunization for prophylactic experiment

C57BL/6 mice were immunized for 3 times from 15 d before tumor bearing at a 5-d interval, then subcutaneously injected with 2×10^4 B16-OVA cells on Day 0. The group, administration dose and monitoring protocol were consistent with the therapeutic anti-tumor treatment.

2.14. Statistical analysis

Based on pilot immunization and tumor treatment studies, we used group sizes of 3 animals per group for *in vivo* evaluation and 6 animals per group for tumor therapy experiments. Statistical analysis was performed using Microsoft Excel and Prism 8.0 (GraphPad). Data were expressed as means ± SEM. Data were analyzed by unpaired two-tailed student t-test. All tests were considered statistically significant if $P < 0.05$
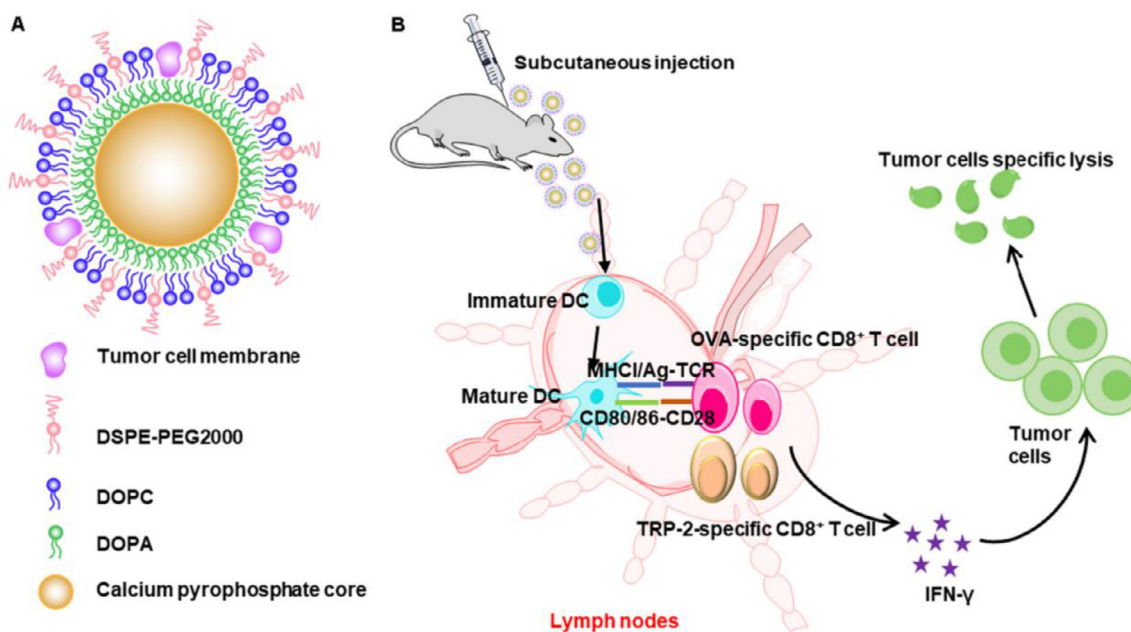
Fig. 1 – Schematic illustration to show the structure of (A) tumor CM@CaPyro NGs and (B) their functions to induce antitumor immunity as a nanovaccine.

(*$P < 0.05$, **$P < 0.01$, ***$P < 0.001$, ****$P < 0.0001$ unless otherwise indicated). The survival rates of the two groups were analyzed using a log-rank test and were considered statistically significant if $P < 0.05$.

3. Results and discussion

3.1. Fabrication and characterization of biomimetic nanovaccine

Fig. 1A shows the structure of calcium pyrophosphate nanovaccine, besides their functions to induce antitumor immunity as a nanovaccine (Fig. 1B). Briefly, the cores of calcium pyrophosphate were formed by reverse microemulsion method, while the nanogranules were obtained by emulsion solvent evaporation method. In such a core-shell structure, DOPA as well as other lipids formed a bilayer together at the surface of CaPyro core. Finally, the tumor cell membrane was loaded into the lipid bilayer by ultrasound fusion.

In terms of characterization, the average size and zeta potential of CaPyro core, CaPyro NGs and CM@CaPyro NGs were determined by DLS (Fig. 2B and S1). The size of CaPyro core was 51.57 ± 0.70 nm, and we found nearly a 10 nm increase of CaPyro NGs in size (61.78 ± 1.20 nm), which was due to the lipid bilayer. And the size of CM@CaPyro NGs slightly enhanced to 64.22 ± 2.10 nm owing to the contribution of CM. As shown in Fig. 2A and Fig. S2, it was also observed that the size of nanogranules through TEM was basically consistent with that of DLS. It was showed that the nanogranules had a good stability within 72 h (Fig. 2C). And, the zeta potential of CaPyro NGs and CM@CaPyro NGs was -24.3 mV and -23.1 mV, respectively (Fig. 2B). Besides,

we performed EDS mapping using a scanning TEM, and the data showed that calcium and phosphorus well co-localized, confirming the formation of CaPyro core via their interaction (Fig. S3). Finally, the loading capacity of cell membrane was found to be 5.58 ± 0.31 µg/mg of CM@CaPyro NGs, and the loading efficiency was $81\% \pm 5\%$. These suggested an effective fusion between cell membrane and lipid bilayers.

3.2. Validation of cancer cell membrane antigen on nanovaccine

In order to prove that the cell membrane was effectively loaded on the nanogranules, we performed SDS-PAGE assay (Fig. 2E). We compared the protein blots after Coomassie blue staining of B16-OVA whole cell lysate, B16-OVA cell membranes, CaPyro NGs and CM@CaPyro NGs. It was found that whole cell lysate, cell membrane and CM@CaPyro NGs showed many similar protein bands, while blank CaPyro NGs did not. To further confirm that antigen proteins were successfully loaded on nanovaccine, the western blot analysis was also conducted. As shown in Fig. 2F, the bands of melanoma tumor associated antigen (gp100) and self-antigen (Trp2) could be obviously observed in whole cell lysate, cell membrane and CM@CaPyro group, respectively. Generally, it was proved here that the biomembrane loading process had basically no effect on the structure of the antigens, suggesting the effective loading of antigen proteins of B16-OVA cell membrane on the nanogranules.

Besides, the band of calreticulin was also found in western blot analysis (Fig. 2F). As we know, the necrosis of cancer cells when exposed to some physical and chemical stress, can induce host to release a type of subcellular components-danger associated molecular patterns (DAMPs), such as heat shock proteins, GRP78 BiP and calreticulin [54]. The band
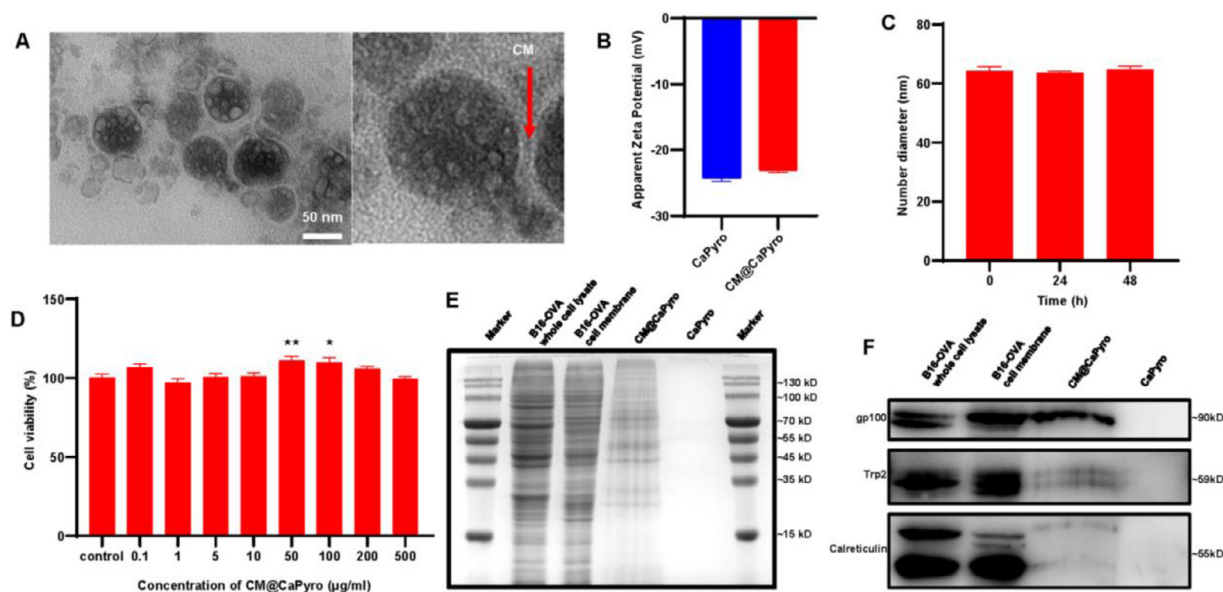
Fig. 2 – Characterization of CM@CaPyro NGs. (A) TEM analysis of CM@CaPyro vaccine. (B) Zeta potential of CaPyro NGs and CM@CaPyro NGs measured by DLS. (C) Stability of CM@CaPyro NGs dispersed in PBS ($n = 3$; mean ± SEM). (D) Cell viability of CM@CaPyro NGs on DC 2.4 cells. (E) SDS-PAGE protein tracking was performed on B16-OVA whole cell lysate, B16-OVA cell membranes, CM@CaPyro NGs and CaPyro NGs, and the protein bands were stained with Coomassie blue. (F) Western blotting detection of tumor-associated antigen (gp100), self-antigen (Trp-2), chaperone protein (calreticulin) on whole B16-OVA cell lysate, B16-OVA cell membranes, CM@CaPyro NGs and CaPyro NGs.

signals of calreticulin which can be seen as DAMPs signals released by necroptotic cancer cells of cell membrane and nanogranules were observed lower than that of B16-OVA cell lysate, we speculated the reason may be that calreticulin is mainly localized on the endoplasmic reticulum [55]. Generally, it was proved here that the proteins on cell membranes were basically transferred onto the nanogranules during the loading procedure, and fortunately, the tumor associated antigen was mostly retained.

3.3. Cytotoxicity assay of biomimetic nanovaccine

The cytotoxicity was measured by CCK-8 assays. Both calcium and pyrophosphate are endogenous which can be found in blood plasma and safely used for organisms [43]. We observed that only high dose of free pyrophosphate was toxic to DC 2.4 cells (Fig. S4A). While, both CaPyro NGs and CM@CaPyro NGs had no antiproliferation effects against DC 2.4 cells in test concentration (Fig. 2D and S4B), revealing that nanoformulation could reduce the toxicity of free drugs. Interestingly, at certain concentrations CaPyro NGs could promote the proliferation of DC 2.4 cells.

3.4. Endocytosis of biomimetic nanovaccine in vitro

Firstly, phagocytosis efficiency of CM@CaPyro NGs was evaluated on DC 2.4 cells and BMDCs using fluorescent labeled cell membranes as controls. The nanogranule dose selected in the current test was based on the previous cytotoxicity assay. As seen in Fig. 3A, the uptake of nanogranules in DC 2.4 cells was time-dependent, which had the strongest mean

fluorescence intensity (MFI) at 24 h, indicating the prolonged antigen and adjuvant release effect of nanogranules [7]. Differently, the internalization reached saturation at 6 h in BMDCs (Fig. 3B), probably because suspended BMDCs could better contact with nanogranules.

Additionally, the uptake efficiency of CM@CaPyro NGs was significantly higher than that of cell membranes (Fig. 3C), according to the finding of confocal laser scanning microscope. Also, we identified the uptake behavior of DC 2.4 cells at different concentrations (Fig. S5A) and temperatures (Fig. S5B). The endocytosis of CM@CaPyro NGs was enhanced as the concentration of nanoparticles was increased (Fig S5A). It indicated that the internalization of CM@CaPyro NGs in DC2.4 cells was concentration-dependent within the range of test concentration. The internalization and processing of nanoparticles into cells is an active process, which requires energy consumption [56]. To determine whether uptake of our nanogranules is mediated by energy-dependent endocytosis, we used low temperature to reduce intracellular energy. Low temperature inhibits the energy production of cells [57]. As shown in Fig S5B, the uptake of CM@CaPyro NGs reduced nearly 43% at 4 °C than that at 37 °C, indicating that the internalization of CM@CaPyro NGs was energy dependent.

3.5. BMDC maturation and antigen-presentation induced by biomimetic nanovaccine in vitro

Antigen uptake, presentation and APCs activation are important stages in immune response [58,59]. The maturation of BMDCs was investigated here using flow cytometry after incubated with nanogranules for 24 h, with LPS as the
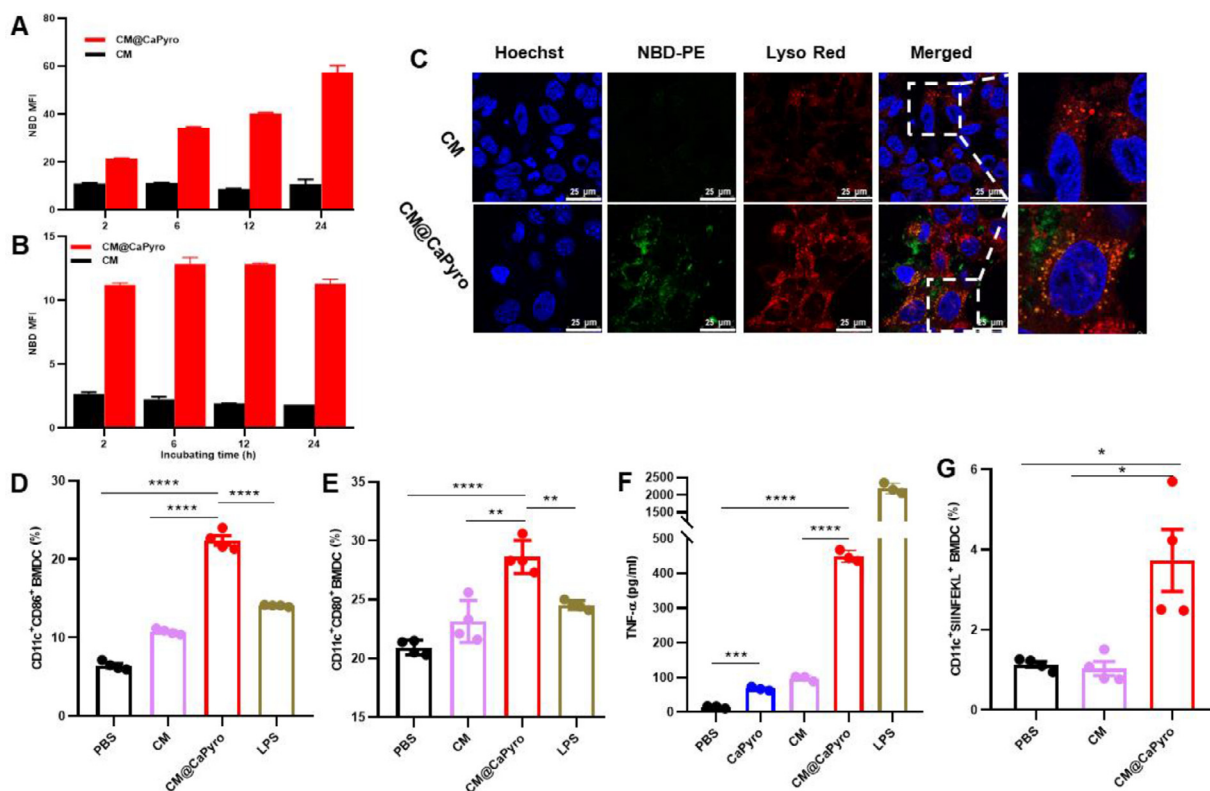
Fig. 3 – Internalization and APCs activation of CM@CaPyro NGs *in vitro*. (A, B) Uptake kinetics of CM@CaPyro NGs by DC 2.4 and BMDCs. (*n* = 3; mean ± SEM). (C) Confocal evaluation of free cell membrane and CM@CaPyro NGs colocalization with lysosomes at 6 h after incubation. Cell membrane and nanogranules labeled by NBD-PE (Green). C57BL/6 mice were subcutaneously injected with nanovaccine. (*n* = 3). (D, E) CD11c, CD86 and CD80 antibodies to characterize the maturation of BMDCs *in vitro* (*n* = 4). (F) TNF-α induced by BMDCs was measured using ELISA (*n* = 3). (G) Levels of antigen presentation on SIINFEKL/H-2Kb in BMDCs induced by cell membrane and CM@CaPyro NGs (*n* = 4). Data are presented as mean ± SEM. *$P <$ 0.05, **$P <$ 0.01, ***$P <$ 0.001, ****$P <$ 0.0001.

positive control. As shown in Fig. 3D and 3E, the exposure to CM@CaPyro NGs significantly enhanced the expression of marker CD86 and CD80 (22.4% and 28.6%), compared with cell membranes (10.8% and 23.2%) and LPS (14.1% and 24.5%). Fig. 3F and Fig. S6 presented the expression levels of TNF-α and IL-12p70 in BMDCs after 24 h stimulation with various groups. Compared to the control group (PBS), the TNF-α and IL-12 in BMDCs induced by treatment with CM@CaPyro NPs showed a 144-fold and a 2-fold increase, respectively. TNF-α and IL-12 are synthesized and released from APCs (such as dendritic cells) to direct cell-mediated immune responses. IL-12 can induce T cell proliferation, NK cell cytolytic activity, and Th1 differentiation. While, TNF-α can trigger pro-inflammatory responses and apoptosis [60]. In short, it demonstrated the effective immunity activity of CM@CaPyro NGs.

The process that DCs activates CD8^{+} T cells by cross-presenting exogenous antigens plays a key role in generating anti-tumor CD8^{+} T cell immunity. Prime CD8^{+} T cells recognize tumor antigens presented on the major histocompatibility complex class I on DCs and are activated to be CTLs through T cell receptor, which then eliminate tumor cells [61]. B16-OVA cell line is an OVA-transfected clone derived from the murine melanoma cell line B16. To verify antigen presentation ability, here we examined whether the model antigen OVA could be presented by BMDCs *in vitro*. The antigen presentation efficiency of treated BMDCs were analyzed by flow cytometry. As shown in Fig. 3G, the percentage of CD11c^{+}SIINFEKL^{+} BMDCs was 3.7%, which is 3.6 times of that in the CM group. So, it was clear that CM@CaPyro NGs could enhanced antigen presentation capacity, but CM was only slightly different from the negative control [32]. Taken together, excellent antigen presentation and APCs activation capabilities of CM@CaPyro NGs provide important potential for subsequent immune effects.

3.6. Lymph nodes retention and APCs activation of biomimetic nanovaccine in vivo

To study the migration and retention characteristics of nanogranules, C57BL/6 mice were injected subcutaneously with CM@CaPyro NGs. Then we measured lymph nodes obtained at different time points by living imaging. Images of isolated draining LNs showed that NGs rapidly accumulated within LNs at 4 h, had strongest signal at 48 h and persisted over 168 h (Fig. 4A & 4B). Compared with other tissues, the highest fluorescence intensity was observed in LNs at 24 h (Fig. 4C). We believe that prolonged retention provides the basis for a long-lasting, sustained immune response.
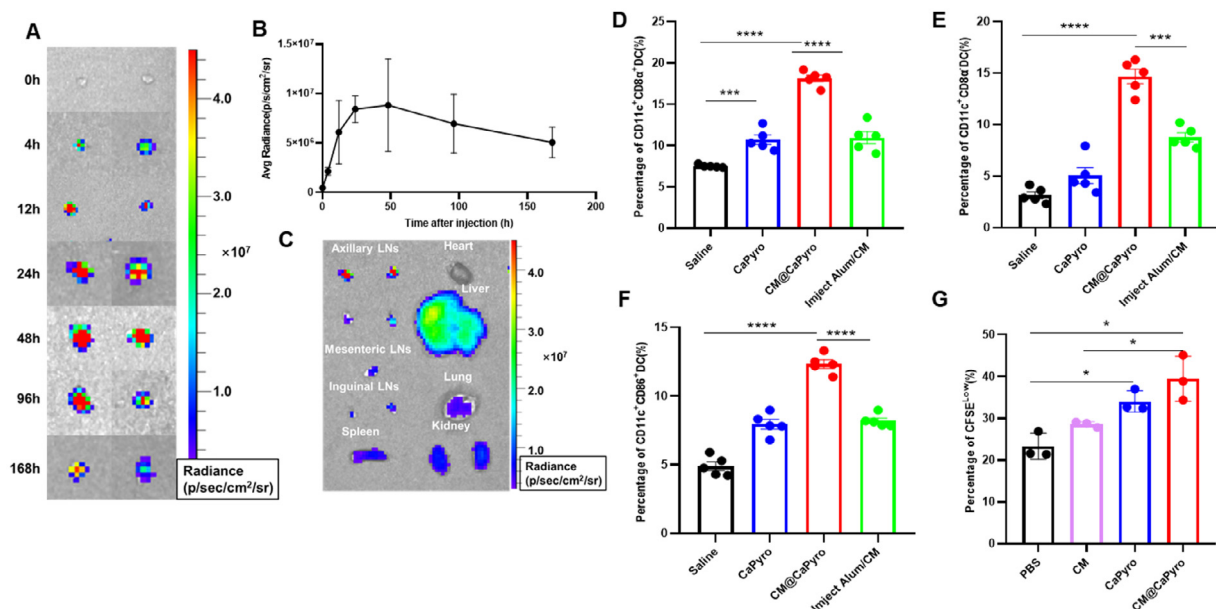
Fig. 4 – Lymph nodes retention and APCs activation of biomimetic nanovaccine *in vivo*. C57BL/6 mice were subcutaneously injected with nanovaccine. (*n* = 3). (A) The representative fluorescence images of the draining LNs in armpit at different time points after immunization. (B) Quantification of average radiance of draining LNs at different time points. (C) Fluorescence images of main organs at 24 h after injection. The proportion of CD8α^+ (D) and CD8α^- (E) DCs in draining LNs (*n* = 5). (F) Using CD11c and CD86 to measure the level of maturation of DCs in draining LNs (*n* = 5). (G) Fluorescence intensity changes of CFSE were detected to evaluate the proliferative effect of CM@CaPyro NGs on BMDCs (*n* = 4). Data are presented as mean ± SEM. *P < 0.05, **P < 0.01, ***P < 0.001, ****P < 0.0001.

According to function and surface markers, DCs are divided into four categories: plasmacyte like DC (pDC), classical DC (cDC), Langerhans cells and monocyte derived DC (moDC). The cDCs are further divided into two subgroups, renamed as cDC1 (CD8α^+DC) and cDC2 (CD8α^- DC) [62]. The cDC1 subset of classical dendritic cells is specialized for priming CD8$^+$ T cell responses through the process of cross-presentation. And the cDC2 lineage can induce functional T follicular helper cells which is a true B cell helper and have a critical role in enhancing humoral immune responses [63]. Here, we prepared single-cell suspensions from lymph nodes, and analyzed the subsets and maturation of DC cells by flow cytometry. As seen in Fig. 4D and 4E, percentage of both CD8α^+ DC and CD8α^- DC aggrandized significantly, increasing 3–5 fold compared to saline group. Also, the expression of surface molecular markers of APCs maturation such as CD86 and CD80 were significantly enhanced. In CM@CaPyro NGs group (Fig. 4F and S9), the CD86 and CD80 expression levels in BMDCs showed an increase to 12.3% and 9.5%, respectively, which was in sharp contrast to the PBS group (~4.9% and ~6.2%) and the Imject Alum/CM group (~8.0% and ~8.5%). These results were consistent with BMDC maturation induced by CM@CaPyro *in vitro*.

3.7. Verification of adjuvant effect of calcium phosphate in BMDCs

In early studies, we found that CaPyro has some proliferative effect on APCs, both CaPyro and CM@CaPyro NGs could promote DC 2.4 cells proliferation within the concentration of 50–200 μg/ml (Fig. 2D and S4), and the proportion of CD11c$^+$ BMDCs in CM@CaPyro NGs group was significantly higher than that in PBS, comparable to the LPS group (Fig. S7).

Based on previous studies, biocompatible calcium phosphate nanoparticles with tunable properties inducing a balanced Th1 and Th2 immune response, possess the potential to act as vaccine adjuvants [35,64]. Proper particle size makes CaPyro nanogranules easier to be engulfed by dendritic cells, resulting in efficient antigen presentation and subsequent adaptive immune response [65,66]. We speculate that CaPyro nanogranules with good biocompatibility as well as similar composition and size can also play an adjuvant role and enhance the immune response.

In order to verify the proliferative effect of CaPyro on APCs, we utilized a CFSE-labeled BMDCs here and analyzed the change in CFSE fluorescence intensity after incubation with the CaPyro NGs and CM@CaPyro NGs for 12 h. CFSE is a good cell marker that can bind to intracellular cytoskeleton proteins. When cells undergo division and proliferation, cytosolic proteins with fluorescence are evenly distributed to second-generation cells, resulting in decrease of cell fluorescence. Consequently, the proportion of CFSE^{LOW} cells in CD11c$^+$ BMDCs was up-regulated in CaPyro and CM@CaPyro NGs groups after 24 h incubation (Fig. 4G and S8). These findings demonstrated that CaPyro had a favorable adjuvant effect in terms of triggering the proliferate of BMDCs.
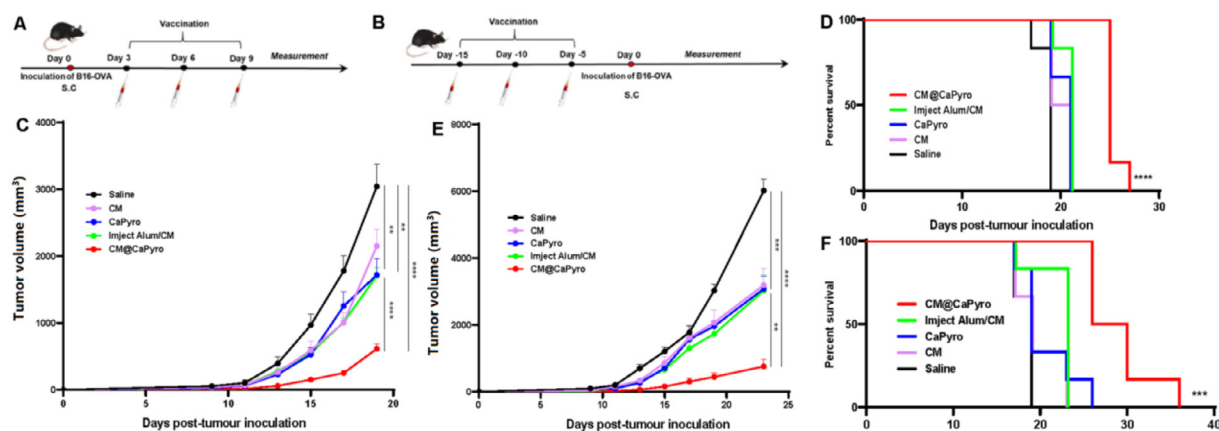
Fig. 5 – The nano vaccine-induced therapeutic and prophylactic immune effects in the B16-OVA model. C57BL/6 mice were subcutaneously injected with 2×10^4 B16-OVA tumor cells ($n = 6$). Tumor volume was recorded every 2 d For therapeutic experiment (A), the mice were immunized with the indicated formulations on Day 3, 6 and 9. (C) Statistical analysis of the tumor growth curves of mice received different treatment. (D) The survival rate of the mice in therapeutic experiment. For prophylactic experiment (B), the mice were immunized with the indicated formulations on Day 15, 10 and 5. (E) Average tumor growth curves of prophylactic experiment, (F) survival rates of prophylactic experiment are shown. Data are presented as mean ± SEM. In survival rate analysis, P values were calculated by Log-rank (Mantel-Cox) Test. *P < 0.05, **P < 0.01, ***P < 0.001, ****P < 0.0001.

3.8. Antineoplastic immune response of biomimetic nanovaccine in vivo

We first assessed the antitumor potential of CM@CaPyro as a therapeutic vaccine. B16-OVA cells were subcutaneously injected into the left armpit of C57BL/6 mice and followed by three subcutaneous immunization with saline, CM, CaPyro, CM@CaPyro and Imject Alum/CM at intervals of 3 d from the third day post tumor inoculation, using CM and traditional adjuvant Imject Alum as positive controls (Fig. 5A). Among all test groups, CM@CaPyro mostly retarded tumor growth (Fig. 5C). Also, the tumors in CaPyro group grew slower than saline group, comparable to that of the Imject Alum/CM group (Fig. 5C), which confirmed the adjuvant effect of CaPyro from another side. Besides, CM@CaPyro actualized the longest median survival of mice (25 d) and the highest survival rate among all treatments (Fig. 5D).

3.9. Prophylactic efficacy of biomimetic nanovaccine in vivo

Then, we hope to know if CM@CaPyro is potential to prevent tumor growth. The C57/BL6 mice were immunized with different formulations 3 times at a 5-d interval from 15 d before tumor inoculation. B16-OVA cells were subcutaneously injected into C57BL/6 mice 5 d after the last immunization (Fig. 5B). It was found that CM@CaPyro group could effectively inhibit tumor progression compared to other groups, and the nanovaccine exhibited the strongest antitumor efficacy compared to all other formulations (Fig. 5E). The median survival of CM@CaPyro group was significantly extended to 28 d (Fig. 5F). Similarly, CaPyro showed some antitumor effects here, which was better than that of the saline group (Fig. 5E and 5F). All these greatly support the feasibility and validity of our design in the use of cancer cell membrane as the tumor-specific antigen, as well as CaPyro NGs as vehicles and the immune adjuvants to further promote vaccination efficacy.

3.10. Stimulation of cytotoxic or infiltrating t lymphocytes by biomimetic nanovaccine in vivo

To reveal the potential mechanism of nanovaccine against tumor progression, immunized mice were sacrificed on Day 5 (for spleen and peripheral blood) and Day 12 (for tumor) after the last immunization. The single-cell suspension of spleen, tumor and peripheral blood was obtained, respectively, and the surface markers CD3, CD4, CD8α were stained with corresponding antibodies. We detected the changes of T lymphocytes proportion by flow cytometry.

CD8$^+$ CTLs are preferred immune cells for targeting cancer [67]. CD8$^+$ T cells possess cytotoxic functions against cancer cells and suppressive effects on regulatory T lymphocytes. Here, the frequency of cytotoxic CD8$^+$ T cells in CD3$^+$ cells in spleen was found to elevate to 29.8% after CM@CaPyro immunization compared with the saline (25.8%) and Imject Alum/CM (27.1%) (Fig. S11A). It is believed that the changes in T cell proportion indicate that vaccine plays an important role and will significantly impact the outcome of treatment [7]. Similarly, the proportion of CD8$^+$ T cells in peripheral blood of immunized group also significantly increased to 30.6%, while the saline group was only 24.1% (Fig. S11C). In tumor, percentage of CD8$^+$ T cells up-regulated 3–4 fold compared to saline group (Fig. S11B).

The CD8/CD4 ratio provides a valuable decision-making indicator for adoptive immunotherapy with or without other conventional therapies such as chemotherapy and/or radiotherapy at any stage of cancer [31,68]. In the therapeutic
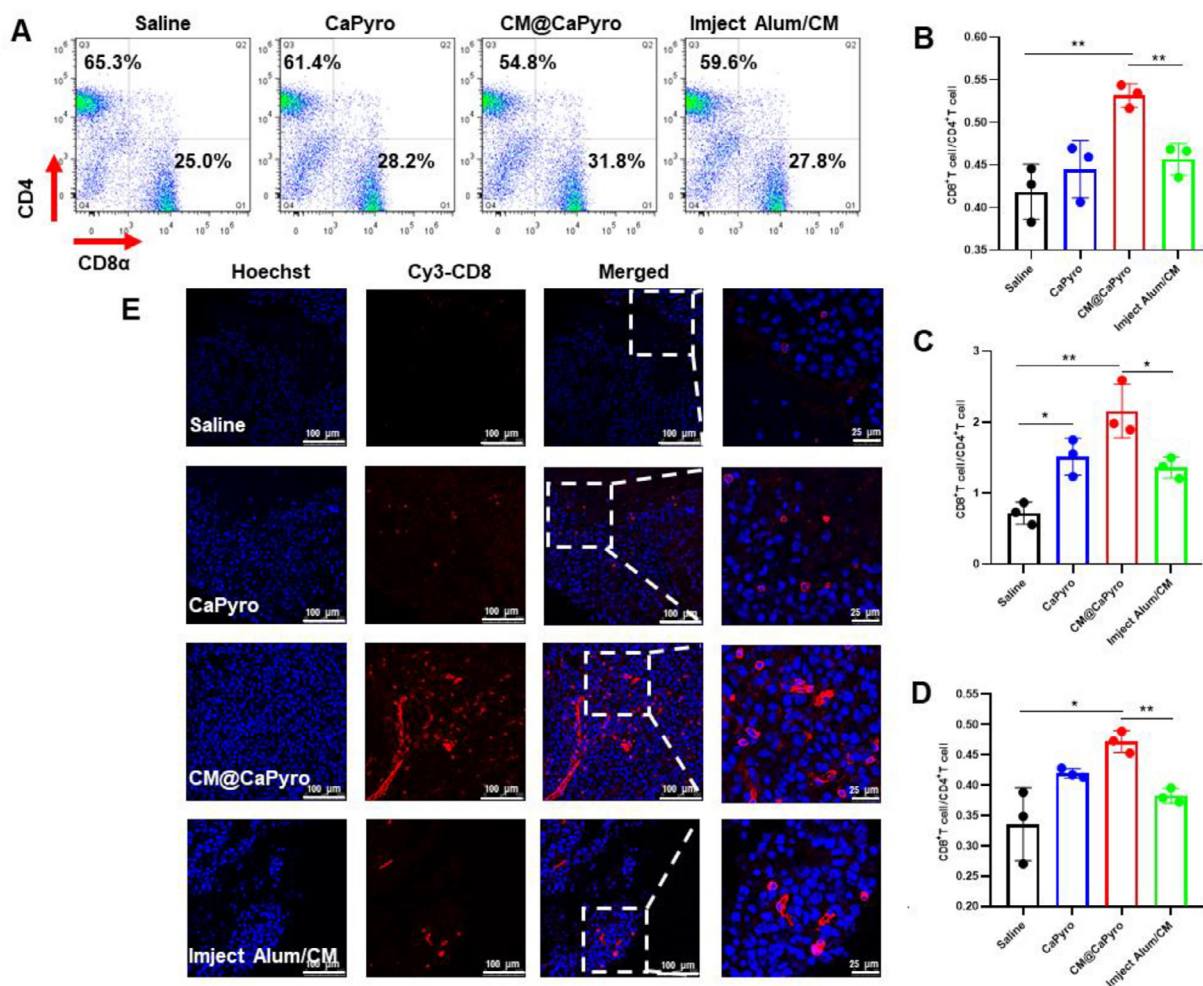
Fig. 6 – Stimulation of T cell responses and tumor-infiltrated CTLs elicited by nanovaccine *in vivo*. To validate the CTL effect generated from CM@CaPyro vaccine, the dosing schedule for mice is the same as that of the therapeutic experiment. The mice were sacrificed on day 14 for spleens and peripheral blood and on day 21 for tumors ($n = 3$). (A, B) The proportion of CD4$^+$ and CD8$^+$ T cells in splenocytes from mice is quantified. The ratio of CD8$^+$ T cells/CD4$^+$ T cells in tumor (C) and peripheral blood (D). (E) Representative immuno-fluorescence assay of CD8$^+$ T cells (red) in B16-OVA melanoma tumors. Data are presented as mean ± SEM. *$P < 0.05$, **$P < 0.01$, ***$P < 0.001$, ****$P < 0.0001$.

test here, the CD8/CD4 ratio observed in the CM@CaPyro group significantly enhanced in the spleen, tumor, and peripheral blood (Fig. 6A, 6B, 6C and 6D). Even compared to the positive control Imject Alum/CM group, the CM@CaPyro vaccine still had extraordinary performance, namely the ratio obviously up-regulated. It was worth mentioning that the ratio of blank CaPyro group without antigen also increased to a certain extent.

To further confirm the activation of T cells, we analyzed the situation of tumor infiltrating CD8$^+$ T lymphocytes using an immunofluorescence assay. More localized CD8$^+$ T cell infiltration often means that tumor is more sensitive to checkpoint blockade therapy and/or therapeutic vaccine treatment, leading to a good prognosis [69,70]. Here, maximum CD8$^+$ T cells infiltration was observed in CM@CaPyro group. CaPyro and Imject Alum/CM groups showed similar infiltration effects, consistent with flow cytometry study. (Fig. 6E)

3.11. Safety and biocompatibility of biomimetic nanovaccine

As mentioned earlier, calcium and pyrophosphate are biocompatibility because both of them are endogenous in plasma [43]. The chemical composition of calcium phosphate nanoparticles is similar to some tissue components of the human body (such as bones, teeth, etc.). Previous studies have shown that CaPyro is safe, nontoxic in the body [71,72] and degradable. To confirm the safety of nanovaccine *in vivo*, here histopathology study was carried out for spleen, kidney, heart, lungs and liver. It was found that there was no obvious change in the tissue structures of these organs. Additionally, the nucleus structure was clear and there was no obvious cell necrosis (Fig. S12). So, it seemed that the vaccine had no obvious toxicity to these organs. Blood routine examination also showed the systemic safety of these formulations (Fig. S13). The body weight of all test mice was measured every

other day during the treatment period, which did not decrease significantly (Fig. S10).

To further demonstrate the safety and biocompatibility of vaccines at the micro level, we observed the effect of nanogranules on major organelles through cell TEM. It was clear that major organelles such as Golgi apparatus, endoplasmic reticulum, mitochondria and cell membranes were not significantly different from the control group (Fig. S14), suggesting the safety of CM@CaPyro vaccine even at the cellular level.

4.   Conclusion

In present study, we have successfully constructed a biomimetic nanovaccine CM@CaPyro using biocompatible carrier materials to load high concentration of antigenic materials. Due to the high heterogeneity and mutation of cancer cells, vaccination based on a single tumor-associated antigen may not be sufficient [73,74]. However, if whole-cell proteins are used as antigens, the therapeutic effect may be affected by a large number of irrelevant proteins in the cells, after all the relevant antigens only account for a small part of the total proteins [73]. Therefore, the use of cell membranes as antigens may be an effective method, because APCs activate immune effects mainly by identifying antigens on tumor cell membranes. Here, we selected B16-OVA tumor cell membrane as the model antigen. We loaded membrane antigens successfully by coating cell membranes onto nanocarriers. It was demonstrated that the tumor cell membranes on nanogranules promoted antigen uptake and presentation (Fig. 3A, 3B and 3G).

Biocompatible drug delivery carriers exhibit higher application value and clinical prospects. We chose calcium and pyrophosphate as the components of nanogranules because of their good biocompatibility and safety [75–77]. The adjuvant effect of calcium phosphate has been well confirmed [28,78–80]. In our study, we also found that CaPyro facilitated the proliferation of APCs to some degree (Fig. 2D and S4). So, in the hope of that the nanocarrier itself as an adjuvant could enhance immune activation, we constructed such a simple and safe vaccine. In the follow-up, we did prove the ability of the calcium pyrophosphate system as a vaccine adjuvant in terms of better immune activation (Figs. 4 and 6, Fig. S8 and S11).

It was found that the nanovaccine designed could accumulate in the draining lymph nodes in large quantities and retain for a relatively long time, suggesting the potential of long-term immunity (Fig. 4A, 4B and 4C). Therapeutic tumor vaccine is an emerging anti-cancer scheme using tumor-associated antigens to promote anti-tumor immune response, and many encouraging progresses have been made [81,82]. As a therapeutic tumor vaccine, the final formulation here showed strong antitumor ability *in vivo* and excellent T lymphocyte activation (Figs. 5 and 6). Not only that, it also showed merits in preventing tumor progression. So, it might be possible for this vaccine system to be further developed into a comprehensive tumor vaccine.

In summary, encapsulating nanogranules with cancer cell membranes is an effective way to introduce multiple membrane antigens to achieve multi-antigen immunity and tumor-specific immunotherapy. The use of carrier particles as adjuvants makes vaccine design simple and controllable. Using biologically derived antigens and biocompatible materials provides a basis for clinical transformation of vaccines. Moreover, the nano system constructed in this study possess adjuvant effect and may be applied to other types of tumors, providing a feasible method for tumor immunotherapy.

Conflicts of interest

The authors report no conflicts of interest. The authors alone are responsible for the content and writing of this article.

Acknowledgments

Supplementary materials

Supplementary material associated with this article can be found, in the online version, at doi:10.1016/j.ajps.2020.06.006.

REFERENCES

[1] Lipson EJ, Forde PM, Hammers H-J, Emens LA, Taube JM, Topalian SL. Antagonists of PD-1 and PD-L1 in cancer treatment. Semin Oncol 2015;42(4):587–600.

[2] Mackall CL. Engineering a designer immunotherapy. Science 2018;359(6379):990–1.

[3] Liu WL, Zou MZ, Liu T, Zeng JY, Li X, Yu WY, et al. Expandable immunotherapeutic nanoplatforms engineered from cytomembranes of hybrid cells derived from cancer and dendritic cells. Adv Mater Weinheim 2019;31(18):e1900499.

[4] Riley R, June C, Langer R, Mitchell M. Delivery technologies for cancer immunotherapy. Nat Rev Drug Discov 2019;18.

[5] Rosenberg SA. IL-2: the first effective immunotherapy for human cancer. J Immunol 2014;192(12):5451–8.

[6] Le DT, Uram JN, Wang H, Bartlett BR, Kemberling H, Eyring AD, et al. PD-1 blockade in tumors with mismatch-repair deficiency. N Engl J Med 2015;372(26):2509–20.

[7] Kang T, Huang Y, Zhu Q, Cheng H, Pei Y, Feng J, et al. Necroptotic cancer cells-mimicry nanovaccine boosts anti-tumor immunity with tailored immune-stimulatory modality. Biomaterials 2018;164:80–97.

[8] Voena C, Chiarle R. Advances in cancer immunology and cancer immunotherapy. Discov Med 2016;21(114):125–33.

[9] Yee C. Adoptive T-cell therapy for cancer: boutique therapy or treatment modality? Clin Cancer Res 2013;19(17):4550–2.

[10] Morgan RA, Dudley ME, Rosenberg SA. Adoptive cell therapy: genetic modification to redirect effector cell specificity. Cancer J 2010;16(4):336–41.

[11] Ochyl LJ, Bazzill JD, Park C, Xu Y, Kuai R, Moon JJ. PEGylated tumor cell membrane vesicles as a new vaccine platform for cancer immunotherapy. Biomaterials 2018;182:157–66.

[12] Sahin U, Derhovanessian E, Miller M, Kloke BP, Simon P, Löwer M, et al. Personalized RNA mutanome vaccines mobilize poly-specific therapeutic immunity against cancer. Nature 2017;547(7662):222–6.

[13] Song Q, Zhang CD, Wu XH. Therapeutic cancer vaccines: from initial findings to prospects. Immunol Lett 2018;196:11–21.

[14] Hu Z, Ott PA, Wu CJ. Towards personalized, tumour-specific, therapeutic vaccines for cancer. Nat Rev Immunol 2018;18(3):168–82.

[15] Jones LH. Recent advances in the molecular design of synthetic vaccines. Nat Chem 2015;7(12):952–60.

[16] Li R, He Y, Zhang S, Qin J, Wang J. Cell membrane-based nanoparticles: a new biomimetic platform for tumor diagnosis and treatment. Acta Pharm Sin B 2018;8(1):14–22.

[17] Ott PA, Hu Z, Keskin DB, Shukla SA, Sun J, Bozym DJ, et al. An immunogenic personal neoantigen vaccine for patients with melanoma. Nature 2017;547(7662):217–21.

[18] Guo Y, Lei K, Tang L. Neoantigen vaccine delivery for personalized anticancer immunotherapy. Front Immunol 2018;9:1499.

[19] Liu J, Miao L, Sui J, Hao Y, Huang G. Nanoparticle cancer vaccines: design considerations and recent advances. Asian J Pharmaceut Sci 2019.

[20] Chen Q, Xu L, Liang C, Wang C, Peng R, Liu Z. Photothermal therapy with immune-adjuvant nanoparticles together with checkpoint blockade for effective cancer immunotherapy. Nat Commun 2016;7:13193.

[21] Banchereau J, Palucka K. Immunotherapy: cancer vaccines on the move. Nat Rev Clin Oncol 2018;15(1).

[22] Khong H, Overwijk WW. Adjuvants for peptide-based cancer vaccines. J Immunother Cancer 2016;4:56.

[23] Exley C, Swarbrick L, Gherardi RK, Authier FJ. A role for the body burden of aluminium in vaccine-associated macrophagic myofasciitis and chronic fatigue syndrome. Med Hypotheses 2009;72(2):135–9.

[24] Tomljenovic L, Shaw CA. Aluminum vaccine adjuvants: are they safe? Curr Med Chem 2011;18(17):2630–7.

[25] Marichal T, Ohata K, Bedoret D, Mesnil C, Sabatel C, Kobiyama K, et al. DNA released from dying host cells mediates aluminum adjuvant activity. Nat Med 2011;17(8):996–1002.

[26] Sun B, Ji Z, Xia T. Aluminum-based nano-adjuvants. In: Bhushan B, editor. Encyclopedia of nanotechnology.. DordrechtNetherlands: Springer; 2016. p. 117–22.

[27] Peer D, Karp JM, Hong S, Farokhzad OC, Margalit R, Langer R. Nanocarriers as an emerging platform for cancer therapy. Nat Nanotechnol 2007;2(12):751–60.

[28] Masson JD, Thibaudon M, Bélec L, Crépeaux G. Calcium phosphate: a substitute for aluminum adjuvants? Expert Rev Vaccines 2017;16(3):289–99.

[29] Goto N, Kato H, Maeyama J, Shibano M, Saito T, Yamaguchi J, et al. Local tissue irritating effects and adjuvant activities of calcium phosphate and aluminium hydroxide with different physical properties. Vaccine 1997;15(12–13):1364–71.

[30] Wang J, Hu X, Xiang D. Nanoparticle drug delivery systems: an excellent carrier for tumor peptide vaccines. Drug Deliv 2018;25(1):1319–27.

[31] Wang K, Wen S, He L, Li A, Li Y, Dong H, et al. "Minimalist" nanovaccine constituted from near whole antigen for cancer immunotherapy. ACS Nano 2018;12(7):6398–409.

[32] Luo M, Wang H, Wang Z, Cai H, Lu Z, Li Y, et al. A STING-activating nanovaccine for cancer immunotherapy. Nat Nanotechnol 2017;12(7):648–54.

[33] Li AW, Sobral MC, Badrinath S, Choi Y, Graveline A, Stafford AG, et al. A facile approach to enhance antigen response for personalized cancer vaccination. Nat Mater 2018;17(6):528–34.

[34] Zhu G, Lynn GM, Jacobson O, Chen K, Liu Y, Zhang H, et al. Albumin/vaccine nanocomplexes that assemble *in vivo* for combination cancer immunotherapy. Nat Commun 2017;8(1):1954.

[35] Lin Y, Wang X, Huang X, Zhang J, Xia N, Zhao Q. Calcium phosphate nanoparticles as a new generation vaccine adjuvant. Expert Rev Vaccines 2017;16(9):895–906.

[36] Hayashi M, Aoshi T, Kogai Y, Nomi D, Haseda Y, Kuroda E, et al. Optimization of physiological properties of hydroxyapatite as a vaccine adjuvant. Vaccine 2016;34(3):306–12.

[37] Li J, Chen YC, Tseng YC, Mozumdar S, Huang L. Biodegradable calcium phosphate nanoparticle with lipid coating for systemic siRNA delivery. J Controlled Release 2010;142(3):416–21.

[38] Kim MG, Park JY, Shon Y, Kim G, Shim G, Oh YK. Nanotechnology and vaccine development. Asian J Pharmaceut Sci 2014;9(5):227–35.

[39] Amenta V, Aschberger K. Carbon nanotubes: potential medical applications and safety concerns. Wiley Interdiscip Rev Nanomed Nanobiotechnol 2015;7(3):371–86.

[40] Choi J, Wang NS. Nanoparticles in Biomedical Applications and Their Safety Concerns. 2011.

[41] Yang Z, Liu ZW, Allaker RP, Reip P, Oxford J, Ahmad Z, et al. A review of nanoparticle functionality and toxicity on the central nervous system. J R Soc Interface 2010;7(Suppl 4):S411–SS22.

[42] Zhu X, Chang Y, Chen Y. Toxicity and bioaccumulation of TiO2 nanoparticle aggregates in Daphnia magna. Chemosphere 2010;78(3):209–15.

[43] Duan X, Chan C, Guo N, Han W, Weichselbaum RR, Lin W. Photodynamic therapy mediated by nontoxic core-shell nanoparticles synergizes with immune checkpoint blockade to elicit antitumor immunity and antimetastatic effect on breast cancer. J Am Chem Soc 2016;138(51):16686–95.

[44] Chen F, Zhu YJ, Zhang KH, Wu J, Wang KW, Tang QL, et al. Europium-doped amorphous calcium phosphate porous nanospheres: preparation and application as luminescent drug carriers. Nanoscale Res Lett 2011;6(1):67.

[45] Altinoğlu EI, Russin TJ, Kaiser JM, Barth BM, Eklund PC, Kester M, et al. Near-infrared emitting fluorophore-doped calcium phosphate nanoparticles for *in vivo* imaging of human breast cancer. ACS Nano 2008;2(10):2075–84.

[46] Barth BM, Sharma R, Altinoğlu EI, Morgan TT, Shanmugavelandy SS, Kaiser JM, et al. Bioconjugation of calcium phosphosilicate composite nanoparticles for selective targeting of human breast and pancreatic cancers *in vivo*. ACS Nano 2010;4(3):1279–87.

[47] He C, Duan X, Guo N, Chan C, Poon C, Weichselbaum RR, et al. Core-shell nanoscale coordination polymers combine chemotherapy and photodynamic therapy to potentiate checkpoint blockade cancer immunotherapy. Nat Commun 2016;7:12499.

[48] Morgan TT, Muddana HS, Altinoglu EI, Rouse SM, Tabaković A, Tabouillot T, et al. Encapsulation of organic molecules in calcium phosphate nanocomposite particles for intracellular imaging and drug delivery. Nano Lett 2008;8(12):4108–15.

[49] Wang Y, Yin S, Zhang L, Shi K, Tang J, Zhang Z, et al. A tumor-activatable particle with antimetastatic potential in breast cancer via inhibiting the autophagy-dependent disassembly of focal adhesion. Biomaterials 2018;168:1–9.

[50] Maitra A. Calcium phosphate nanoparticles: second-generation nonviral vectors in gene therapy. Expert Rev Mol Diagn 2005;5(6):893–905.

[51] Srinivasu B, Mitra G, Muralidharan M, Srivastava D, Pinto J, Thankachan P, et al. Beneficiary effect of nanosizing Ferric Pyrophosphate as food fortificant in Iron Deficiency Anemia:

evaluation of bioavailability, toxicity and plasma biomarker. RSC Adv 2015;5.

[52] Liu D, Poon C, Lu K, He C, Lin W. Self-assembled nanoscale coordination polymers with trigger release properties for effective anticancer therapy. Nat Commun 2014;5:4182.

[53] Kroll AV, Fang RH, Jiang Y, Zhou J, Wei X, Yu CL, et al. Nanoparticulate delivery of cancer cell membrane elicits multiantigenic antitumor immunity. Adv Mater Weinheim 2017;29(47).

[54] Aaes TL, Kaczmarek A, Delvaeye T, De Craene B, De Koker S, Heyndrickx L, et al. Vaccination with necroptotic cancer cells induces efficient anti-tumor immunity. Cell Rep 2016;15(2):274–87.

[55] Yang Y, Ma F, Liu Z, Su Q, Liu Y, Liu Z, et al. The ER-localized Ca-binding protein calreticulin couples ER stress to autophagy by associating with microtubule-associated protein 1A/1B light chain 3. J Biol Chem 2019;294(3):772–82.

[56] Vácha R, Martinez-Veracoechea FJ, Frenkel D. Receptor-mediated endocytosis of nanoparticles of various shapes. Nano Lett 2011;11(12):5391–5.

[57] Zhu J, Liao L, Zhu L, Zhang P, Guo K, Kong J, et al. Size-dependent cellular uptake efficiency, mechanism, and cytotoxicity of silica nanoparticles toward HeLa cells. Talanta 2013;107:408–15.

[58] Whitton JL. An overview of antigen presentation and its central role in the immune response. Curr Top Microbiol Immunol 1998;232.

[59] Banchereau J, Steinman RM. Dendritic cells and the control of immunity. Nature 1998;392(6673):245–52.

[60] Hanlon AM, Jang S, Salgame P. Signaling from cytokine receptors that affect TH1 responses. Front Biosci 2002;7:d1247–d1d54.

[61] Fu C, Jiang A. Dendritic cells and CD8 T cell immunity in tumor microenvironment. Front Immunol 2018;9:3059.

[62] Theisen D, Murphy K. The role of cDC1s: CD8 T cell priming through cross-presentation. F1000Res 2017;6:98.

[63] Shin C, Han JA, Choi B, Cho YK, Do Y, Ryu S. Intrinsic features of the CD8α(-) dendritic cell subset in inducing functional T follicular helper cells. Immunol Lett 2016;172:21–8.

[64] Jiang D, Premachandra GS, Johnston C, Hem SL. Structure and adsorption properties of commercial calcium phosphate adjuvant. Vaccine 2004;23(5):693–8.

[65] Shah RR, O'Hagan DT, Amiji MM, Brito LA. The impact of size on particulate vaccine adjuvants. Nanomedicine (Lond) 2014;9(17):2671–81.

[66] Kuroda E, Coban C, Ishii KJ. Particulate Adjuvant and Innate Immunity: past Achievements, Present Findings, and Future Prospects. Int Rev Immunol 2013;32(2):209–20.

[67] Farhood B, Najafi M, Mortezaee K. CD8+ cytotoxic T lymphocytes in cancer immunotherapy: a review. J Cell Physiol 2019;234(6):8509–21.

[68] Shindo G, Endo T, Onda M, Goto S, Miyamoto Y, Kaneko T. Is the CD4/CD8 Ratio an Effective Indicator for Clinical Estimation of Adoptive Immunotherapy for Cancer Treatment? J Cancer Ther 2013;4(8):9.

[69] Spranger S, Gajewski TF. Impact of oncogenic pathways on evasion of antitumour immune responses. Nat Rev Cancer 2018;18(3):139–47.

[70] Hu WH, Miyai K, Cajas-Monson LC, Luo L, Liu L, Ramamoorthy SL. Tumor-infiltrating CD8(+) T lymphocytes associated with clinical outcome in anal squamous cell carcinoma. J Surg Oncol 2015;112(4):421–6.

[71] Muddana HS, Morgan TT, Adair JH, Butler PJ. Photophysics of Cy3-encapsulated calcium phosphate nanoparticles. Nano Lett 2009;9(4):1559–66.

[72] Sokolova V, Knuschke T, Kovtun A, Buer J, Epple M, Westendorf AM. The use of calcium phosphate nanoparticles encapsulating Toll-like receptor ligands and the antigen hemagglutinin to induce dendritic cell maturation and T cell activation. Biomaterials 2010;31(21):5627–33.

[73] Fang RH, Hu C-MJ, Luk BT, Gao W, Copp JA, Tai Y, et al. Cancer cell membrane-coated nanoparticles for anticancer vaccination and drug delivery. Nano Lett 2014;14(4):2181–8.

[74] Lollini PL, Cavallo F, Nanni P, Forni G. Vaccines for tumour prevention. Nat Rev Cancer 2006;6(3):204–16.

[75] de Oliveira NG, de Souza Araújo PR, da Silveira MT, Sobral APV, Carvalho MdV. Comparison of the biocompatibility of calcium silicate-based materials to mineral trioxide aggregate: systematic review. Eur J Dent 2018;12(2):317–26.

[76] Pujari-Palmer M, Pujari-Palmer S, Lu X, Lind T, Melhus H, Engstrand T, et al. Pyrophosphate stimulates differentiation, matrix gene expression and alkaline phosphatase activity in osteoblasts. PLoS ONE 2016;11(10):e0163530.

[77] Link DP, van den Dolder J, van den Beucken JJJP, Cuijpers VM, Wolke JGC, Mikos AG, et al. Evaluation of the biocompatibility of calcium phosphate cement/PLGA microparticle composites. J Biomed Mater Res Part A 2008;87A(3):760–9.

[78] Habraken W, Habibovic P, Epple M, Bohner M. Calcium phosphates in biomedical applications: materials for the future? Materials Today 2015;19.

[79] Saeed MI, Omar AR, Hussein MZ, Elkhidir IM, Sekawi Z. Systemic antibody response to nano-size calcium phospate biocompatible adjuvant adsorbed HEV-71 killed vaccine. Clin Exp Vaccine Res 2015;4(1):88–98.

[80] Salim M, Issa A, Farrag AR, Zedan H, Mohamed A. Ultrastructural and morphometric effect of aluminum phosphate and calcium phosphate nanoparticles as adjuvants in vaccinated mice. J Arab Soc Med Res 2016;11:22.

[81] Aldous AR, Dong JZ. Personalized neoantigen vaccines: a new approach to cancer immunotherapy. Bioorg Med Chem 2018;26(10):2842–9.

[82] Nguyen T, Urban J, Kalinski P. Therapeutic cancer vaccines and combination immunotherapies involving vaccination. Immunotargets Ther 2014;3:135–50.